ORBITS NEAR CRITICAL INCLINATION, INCLUDING LUNISOLAR PERTURBATIONS

MICHAEL E. HOUGH

The Analytic Sciences Corporation, Reading, MA. 01867

(Received 21 January, 1980; Accepted 12 September, 1980)

Abstract. An improved theory is presented of long period perigee motion for orbits near the critical inclinations 63.4° and 116.6°. Inclusion of lunisolar perturbations and *all* measured zonal harmonic coefficients from a recent Earth model are significant improvements over existing theories. Phase portraits are used to depict the interaction between eccentricity magnitude and argument of perigee. The Hamiltonian constant can be chosen as the parameter to display a family of phase plane trajectories consisting of libration, circulation, and asymptotic motion along separatrices near equilibrium points. A two parameter family of phase portraits is defined by the other two integrals, the average semimajor axis and component of angular momentum resolved along the Earth's polar axis. There are regions of the parameter space where the stability and total number of equilibria can change, or two separatrices can coalesce. These phenomena signal large qualitative changes in phase portrait topology. Numerical studies show that lunisolar perturbations control stability of equilibria for orbits with semimajor axes exceeding 1.4 Earth radii. Moreover, a theory which includes lunisolar perturbations predicts larger maximum fluctuations in eccentricity and faster oscillations near stable equilibria compared to a theory which models only the zonal harmonics.

1. Introduction

Since the first artificial satellite was launched in 1957, many authors have investigated the long period dynamics of orbits critically inclined at 63.4° and 116.6°. If gravitational perturbations due to the geopotential alone are considered and if tesseral and sectorial harmonic resonances are avoided, it is well known that only the zonal harmonics cause secular and long period perigee fluctuations. Among those who first reported results on the 'main problem' (J_2 and J_4 only) were Garfinkel (1960), Hori (1960), Petty and Breakwell (1960), and Hagihara (1961). The averaged Hamiltonian expanded about the critical inclinations revealed very slow (on the order of a century) simple pendulum-type oscillations in eccentricity magnitude and argument of perigee. Garfinkel (1973) developed analytic solutions of the main problem in terms of elliptic functions.

In other refinements of the theory, the effect of J_6 was analyzed by Aoki (1963a) whereas Kozai (1961) and Aoki (1963b) included the odd zonal harmonics J_3 and J_5. For orbits with small and moderate eccentricities, not more than five phase plane equilibria were predicted. In a recent paper treating nearly circular orbits and taking all the zonal harmonics into account, Jupp (1980) identified six possible phase portraits. For orbits with large eccentricities under the influence of the zonal harmonics through J_5, Jupp (1975) predicted seven phase plane equilibria for certain non-collision orbits with eccentricities exceeding $\sqrt{6/13}$ (semimajor axes necessarily larger than 3 Earth radii).

Celestial Mechanics **25** (1981) 111–136. 0008–8714/81/0252–0111$03.90.

All of these investigations neglected the secular and long period perigee fluctuations caused by lunar and solar gravitation. Results on related critical inclination problems reported by Hensley and Breakwell (1967) and Vagners (1967) indicate a significant third body perturbation at high altitudes, especially for orbits with large eccentricities. As this paper will show, lunisolar perturbations have a significant impact upon the long period perigee dynamics of subsynchronous Earth orbits near critical inclination. Orbits with small and large eccentricities are considered. Moreover, the zonal harmonic expansion of the geopotential includes *all* measured zonal harmonic coefficients from a recent Earth model.

Aside from the introductory and concluding sections, this paper has four main parts (Sections 2–5). Section 2 discusses how the method of averaging (Brouwer and Clemence, 1961) was used to eliminate short and intermediate period fluctuations from the Hamiltonian. Using the averaged Hamiltonian thus obtained, Section 3 discusses how phase plane methods were used to analyze the long period perigee motions. It is shown that changes in infinitesimal stability and separatrix coalescence cause large qualitative changes in phase plane topology. In Sections 4 and 5, two families of phase plane portraits are compared to illustrate the impact of lunisolar perturbations. If the zonal harmonics only are modeled (Section 4), it is shown that the results are sensitive to the total number of zonal harmonics retained. Comparisons are made with the small eccentricity results of Aoki (1963b) and with the large eccentricity results of Jupp (1975). Section 5 discusses how the lunisolar perturbations completely change the foregoing results, particularly the possible types of phase plane behavior.

2. Development of the Averaged Hamiltonian

At the critical inclinations 63.4° and 116.6°, the average perigee location is unchanged to first-order in J_2 by Earth oblateness. Near the critical inclinations, second-order north-south gravitational forces cause slow changes in the perigee distance and angular location of perigee (perigee resonance). These forces arise because of the Earth's distortion from an oblate spheroid, the Moon, and the Sun.

Non-gravitational forces caused by atmospheric drag and solar radiation pressure can disrupt perigee resonance. For example, atmospheric drag will cause any orbit with perigee altitude less than 700 km to decay. An accurate drag model takes into consideration the geophysics of the upper atmosphere and the attitude dynamics of the spacecraft. It is therefore beyond the scope of this paper to model drag. Consequently, the results apply only to orbits with perigees higher than 700 km. Solar radiation pressure causes long period and, if the orbit is shadowed, secular changes in the perigee. These effects are pronounced at altitudes exceeding 1000 km, particularly for balloon-type satellites. Moreover, the reflective properties and attitude dynamics of the satellite can, together with the Earth's shadow, modulate the amplitude and frequency of the solar pressure force which, if properly rectified, can

also disrupt resonance. Solar pressure effects upon perigee resonance will be examined in a future paper dealing with Sun synchronous orbits near the critical inclination 116.6^0.

The methods of Hamiltonian mechanics are used because only conservative effects are modeled. The second-order Hamiltonian may be written as a sum of negative potential energies:

$$H_2 = -U_\oplus - U_\leftmoon - U_\odot. \tag{1}$$

$U_\oplus$ models terrestrial gravitation and is written (Kaula, 1966):

$$U_\oplus = \frac{\mu_\oplus}{r}\left\{ - \sum_{n\geqslant 2} J_n \left(\frac{R_\oplus}{r}\right)^n P_n(S(\delta)) + \right.$$

$$\left. + \sum_{n\geqslant 2} \sum_{m=1}^{n} J_{nm}\left(\frac{R_\oplus}{r}\right)^n P_{nm}(S(\delta))C(m(\alpha - \theta_\oplus - \lambda_{nm}))\right\}. \tag{2}$$

where α is the right ascension and δ is the declination of the satellite in an Earth-centered inertial frame. $S(\cdot)$ and $C(\cdot)$ are abbreviations for $\sin(\cdot)$ and $\cos(\cdot)$. It is noteworthy that $U_\oplus$ attenuates with increasing radial distance r, where $R_\oplus$ is the Earth's equatorial radius. The zonal harmonic coefficient J_n is the amplitude of pure latitudinal variations in the geopotential modeled by the Legendre polynomial $P_n(\cdot)$. The other terms model longitudinal variations. J_{nm} represents a tesseral ($n \neq m$) or a sectorial ($n = m$) harmonic coefficient. $P_{nm}(\cdot)$ is an associated Legendre polynomial. The Greenwich hour angle $\theta_\oplus$ appears in the same argument with the satellite right ascension and the constant phase λ_{nm} because longitudinal variations are carried East with the Earth as it rotates on its axis.

Third body disturbing potentials may also be expressed in terms of spherical harmonics of the satellite and third body. The lunar potential $U_\leftmoon$ (Giacaglia, 1973) and the solar potential $U_\odot$ (Kozai, 1973) are written:

$$U_\leftmoon = \frac{\mu_\leftmoon}{r_\leftmoon}\left\{1 + \sum_{n\geqslant 2}\left(\frac{r}{r_\leftmoon}\right)^n \left[P_n(S(\delta))P_n(S(\delta_\leftmoon)) + \right.\right.$$

$$\left.\left. + 2\sum_{m=1}^{n} \frac{(n-m)!}{(n+m)!} P_{nm}(S(\delta))P_{nm}(S(\delta_\leftmoon))C(m(\alpha - \alpha_\leftmoon))\right]\right\},$$

$$U_\odot = \frac{\mu_\odot}{r_\odot}\left\{1 + \sum_{n\geqslant 2}\left(\frac{r}{r_\odot}\right)^n \left[P_n(S(\delta))P_n(S(\delta_\odot)) + \right.\right.$$

$$\left.\left. + 2\sum_{m=1}^{n} \frac{(n-m)!}{(n+m)!} P_{nm}(S(\delta))P_{nm}(S(\delta_\odot))C(m(\alpha - \alpha_\odot))\right]\right\}. \tag{3}$$

where $(\alpha_\leftmoon, \delta_\leftmoon)$ and $(\alpha_\odot, \delta_\odot)$ are the (right ascension, declination) of the Moon and Sun, respectively. Significantly, both $U_\leftmoon$ and $U_\odot$ amplify with increasing radial distance r. In order that these disturbing potentials remain second-order with

increasing semimajor axis, an upper semimajor axis limit of 3 Earth radii will arbitrarily be imposed (Section 5). Under these circumstances, it is meaningful to truncate $U_\odot$ at $n = 2$ and $U_\mathbb{C}$ at $n = 4$. In other words, the lunar and solar gravity gradients ($n = 2$) and two higher order lunar gradients are retained.

The Sun and Moon also raise bodily and oceanic tides on the Earth, thereby affecting the geopotential and hence the orbit dynamics. Tides can be modeled as corrections to the zonal, tesseral, and sectorial terms in $U_\oplus$. According to Lange *et al.* (1969), corrections to the zonal terms, for example, are comparable to the uncertainties in the estimates of the zonal harmonic coefficients. Hence, tidal effects are third-order in J_2 and not modeled.

The second-order secular and long period Hamiltonians may be extracted from (1) using Von Zeipel's method (Brouwer and Clemence, 1961). It will later be shown (Sections 4 and 5) that long period perigee oscillations are very slow, of the order one hundred years. Averaging the Hamiltonian eliminates short and intermediate period fluctuations which are much faster than perigee oscillations. If other resonances (e.g. tesseral resonance) exist, the argument of perigee may not be the only slow variable. Under these circumstances, the averages performed here must be modified to include the additional resonant terms. However, the following analysis assumes that these other resonances have been avoided.

The geopotential is averaged over the satellite mean anomaly and ascending node, rendering the conjugate DeLaunay momenta L and H constants of the motion.

$$L = \sqrt{\mu_\oplus a}, \qquad H = L\sqrt{1 - e^2}C(i). \tag{4}$$

The constancy of L is clearly equivalent to the constancy of the average semimajor axis a. Moreover, fluctuations in the average eccentricity e are accompanied by fluctuations in the average inclination i such that the polar angular momentum H is conserved. These averages eliminate the tesseral and sectorial harmonic terms in (2). The lunisolar potential is also averaged over the satellite mean anomaly (preserving the constancy of L), and over the lunar and apparent solar orbital motions. Despite these averages, the lunar potential is time dependent due to the motion of the lunar argument of perigee and ecliptic lunar ascending node. These lunar elements precess due to solar gravity gradient torques on the lunar orbit. The lunar argument of perigee completes one cycle in 8.9 yrs. Lunar nodal precession causes 18.6-year periodic fluctuations in the equatorial elements of the lunar orbit plane. Averaging $U_\mathbb{C}$ over these cycles eliminates all remaining explicit time dependence from the Hamiltonian, rendering it a constant of the motion. Moreover, averaging over lunar perigee precession eliminates the $n = 3$ term in the expansion (3) of $U_\mathbb{C}$.

Secular and long period terms in the second-order Hamiltonian come from the Legendre polynomial terms ($m = 0$) in the terrestrial (2) and third body (3) disturbing potentials. The secular term $\bar{H}_2$ and the long period term H_2^* have the forms:

$$\bar{H}_2(L, G, H) = \left(\frac{\mu_\oplus}{L}\right)^2 \sum_{\substack{M=0,2,4\cdots \\ m=0}} A_{Mm}(L, G, H)e^M,$$

$$H_2^*(L, G, H, g) = \left(\frac{\mu_\oplus}{L}\right)^2 \left\{ \sum_M \sum_m {}_{\text{ODD}} B_{Mm}(L, G, H) e^M S(mg) + \right.$$
$$\left. + \sum_M \sum_m {}_{\text{EVEN}} C_{Mm}(L, G, H) e^M C(mg) \right\}.$$

The coefficients A_{Mm} and C_{Mm} contain even-order zonal harmonics and lunisolar perturbations. The coefficients B_{Mm} contain odd-order zonal harmonics only. All the coefficients depend on the parametric constants L and H, and the fluctuating orbital angular momentum G. It will subsequently be shown that these Hamiltonian coefficients may be meaningfully approximated as being constants.

At the critical inclinations:

$$(\bar{H}_1)_{G_c} \triangleq \frac{\partial \bar{H}_1}{\partial G}\bigg|_{G_c} = -\frac{3}{4}\left(\frac{\mu_\oplus}{L}\right)^2 J_2 \left(\frac{R_\oplus}{a}\right)^2 \left(\frac{L}{G_c}\right)^3 \left[1 - 5\left(\frac{H}{G_c}\right)^2\right] \frac{1}{G_c} = 0,$$
$$\left(\frac{H}{G_c}\right)^2 = \frac{1}{5}, \quad G_c = \pm\sqrt{5}H = L\sqrt{1 - e_c^2} \tag{5}$$

Following Garfinkel (1960), the averaged Hamiltonian is expanded about $G = G_c$ as follows:

$$\mathcal{H} \cong \{\tfrac{1}{2}(\bar{H}_1)_{G_c G_c}(G - G_c)^2 + [\bar{H}_2(L, G_c, H) + H_2^*(L, G_c, H, g)]\} +$$
$$+ \{(\bar{H}_1)_{G_c G_c G_c}(G - G_c)^3 + [(\bar{H}_2)_{G_c} + (H_2^*)_{G_c}](G - G_c)\}. \tag{6}$$

If the second-order Hamiltonian and all its partial derivatives are $0(J_2^2)$, it is clear that the quantity $(G - G_c)/G_c$ is at most $0(\sqrt{J_2})$ during libration (Garfinkel, 1960). It then follows that the first-bracketed term in (6) is the dominant term $(0(J_2^2))$, whereas the second-bracketed term is a higher-order term $(0(J_2^{5/2}))$ and therefore negligible. It is noteworthy that the lunisolar perturbations do not remain $0(J_2^2)$ with increasing semimajor axis. For example, the lunisolar terms are $0(J_2)$ for an orbit with synchronous semimajor axis 6.6 Earth radii, necessitating separate treatment. Since semimajor axes below 3 Earth radii are under consideration (as noted earlier), only the dominant term in (6) need be retained.

Hamiltonian dependence on G occurs in the coefficients A_{Mm}, B_{Mm}, and C_{Mm}, and in powers of eccentricity e^M appearing explicitly. If the latter terms are expanded about $G = G_c$, the higher-order term in (6) will contain a term that is $0(J_2^2)$ whenever the eccentricity is $0(\sqrt{J_2})$ or smaller. For example, $(H_2^*)_G$ would contain $(1/e)S_g$ if the eS_g term is differentiated. However, if only the Hamiltonian coefficients are expanded, the higher-order term is $0(J_2^{5/2})$ even for very small eccentricities. Accordingly, (i) only the coefficients are evaluated at $G = G_c$ in the dominant term (rendering them constants), and (ii) only the coefficients are differentiated in $(\bar{H}_2)_G$ and $(H_2^*)_G$. Explicit powers of eccentricity (e.g. e, e^2, e^3, e^4, etc.) are allowed to fluctuate.

The retained dominant term of (6) is now written in ascending powers of eccentricity:

$$\tfrac{1}{2}(\bar{H}_1)_{G_cG_c}(G-G_c)^2 \cong -\frac{3}{16}\left(\frac{\mu_\oplus}{L}\right)^2 J_2\left(\frac{R_\oplus}{a}\right)^2\left(\frac{L}{G_c}\right)^7(e^2-e_c^2)^2, \tag{7A}$$

$$\bar{H}_2(L, G_c, H) \cong \left(\frac{\mu_\oplus}{L}\right)^2\{A_{00}(L, G_c, H) - \tfrac{1}{2}A_{20}(L, G_c, H)e^2 - A_{40}(L, G_c, H)e^4\}, \tag{7B}$$

$$H_2^*(L, G_c, H, g) \cong \left(\frac{\mu_\oplus}{L}\right)^2\{-[2B_{11}(L, G_c, H) + B_{31}(L, G_c, H)e^2]eS(g) + [C_{22}(L, G_c, H) + C_{42}(L, G_c, H)e^2]e^2C(2g) + B_{33}(L, G_c, H)e^3S(3g) - C_{44}(L, G_c, H)e^4C(4g)\}. \tag{7C}$$

Equations (7) are truncated at the fourth power of eccentricity despite the fact that the eccentricity can be large. (For example, e_c is 0.63 for an orbit with semimajor axis 3 Earth radii and lowest permissible perigee altitude of 700 km.) The rationale for performing this truncation is that terms proportional to $J_2(e^2-e_c^2)^3$ may be neglected in (7A) on the grounds that only the eccentricity *difference* $(e-e_c)$, rather than e or e_c individually, need remain small. Moreover, the ratio of the (neglected) $B_{51}(G_c)e^5$ term to the (retained) $B_{51}(G_c)e^3$ term in (7C) never exceeds $0(\sqrt{J_2})$ for semimajor axes less than 3 Earth radii. Formulae for the nine Hamiltonian coefficients in (7B) and (7C) appear in Appendix A. Although J_3 appears in B_{11}, the amplitude of the J_3 inclination function is identically zero at the critical inclinations. (A term proportional to $J_3(G-G_c)eS_g$ appears in the neglected higher-order term in (6).) The expanded first-order secular term (7A) is incorporated in (7B) by modifying the second-order secular coefficients (hence the tildes):

$$\tfrac{1}{2}(\bar{H}_1)_{G_cG_c}(G-G_c)^2 + \tilde{H}_2(L, G_c, H) = \left(\frac{\mu_\oplus}{L}\right)^2\{\tilde{A}_{00}(L, G_c, H) - \tfrac{1}{2}\tilde{A}_{20}(L, G_c, H)e^2 - \tilde{A}_{40}(L, G_c, H)e^4\}$$

$$\tilde{A}_{00}(L, G_c, H) \triangleq A_{00}(L, G_c, H) - \tfrac{3}{16}J_2\left(\frac{R_\oplus}{a}\right)^2\left(\frac{L}{G_c}\right)^7 e_c^4$$

$$\tilde{A}_{20}(L, G_c, H) \triangleq A_{20}(L, G_c, H) - \tfrac{3}{4}J_2\left(\frac{R_\oplus}{a}\right)^2\left(\frac{L}{G_c}\right)^7 e_c^2$$

$$\tilde{A}_{40}(L, G_c, H) \triangleq A_{40}(L, G_c, H) + \tfrac{3}{16}J_2\left(\frac{R_\oplus}{a}\right)^2\left(\frac{L}{G_c}\right)^7. \tag{8}$$

The well known Von Zeipel correction terms proportional to J_2^2 (Brouwer and Clemence, 1961) are incorporated in A_{00} and C_{22} (Appendix A).

3. Analysis of the Long Period Dynamics

The complicated interactions between the eccentricity magnitude and argument of perigee are best visualized in the modified phase plane (rather than the more conventional momentum-coordinate plot) whose coordinates are:

$$\xi = eC(g), \quad \eta = eS(g). \tag{9}$$

In this representation, the ξ-direction is toward the ascending node of the orbit with the argument of perigee measured positive counterclockwise along the orbit. The η-axis is always in the northern hemisphere. Curves in the $\xi\eta$ plane, which is the plane of the orbit, trace the locus of the tip of the eccentricity vector moving under the influence of the Earth zonal harmonic and lunisolar gravitational fields.

The Hamiltonian is a quartic polynomial in ξ and η:

$$-\mathscr{H}(\xi, \eta) = \xi^2[\beta\xi^2 + P_2(\eta)] + P_4(\eta), \tag{10}$$

where P_2 is a quadratic polynomial in η given by:

$$\begin{aligned} &P_2(\eta) = \Omega_2\eta^2 + \Omega_1\eta + \Omega_0, \\ &\Omega_2 = 2[\tilde{A}_{40} - 3C_{44}], \quad \Omega_1 = B_{31} - 3B_{33}, \quad \Omega_0 = \tfrac{1}{2}\tilde{A}_{20} - C_{22}, \end{aligned} \tag{11}$$

whereas P_4 is a quartic polynomial in η given by:

$$\begin{aligned} &P_4(\eta) = \alpha_4\eta^4 + \alpha_3\eta^3 + \alpha_2\eta^2 + \alpha_1\eta + \alpha_0, \\ &\alpha_4 = \tilde{A}_{40} + C_{42} + C_{44}, \quad \alpha_3 = B_{31} + B_{33}, \quad \alpha_2 = \tfrac{1}{2}\tilde{A}_{20} + C_{22}, \\ &\alpha_1 = 2B_{11}, \quad \alpha_0 = \tilde{A}_{00}, \end{aligned} \tag{12}$$

and β is a constant given by:

$$\beta = \tilde{A}_{40} - C_{42} + C_{44}. \tag{13}$$

All the Hamiltonian coefficients are evaluated at $G = G_c$.

The ξ and η differential equations are:

$$\frac{d\xi}{d\tau} = \sqrt{(1 - \xi^2 - \eta^2)}\frac{\partial\mathscr{H}}{\partial\eta}, \quad \frac{d\eta}{d\tau} = -\sqrt{(1 - \xi^2 - \eta^2)}\frac{\partial\mathscr{H}}{\partial\xi}, \quad \tau = nt. \tag{14}$$

Equilibrium solutions satisfy:

$$-\frac{\partial\mathscr{H}}{\partial\eta} = \xi^2 P_2'(\eta) + P_4'(\eta) = 0, \tag{15A}$$

$$-\frac{\partial\mathscr{H}}{\partial\xi} = 2\xi[2\beta\xi^2 + P_2(\eta)] = 0. \tag{15B}$$

Primes denote differentiation with respect to η. Since the coefficients are constants,

they are *not* differentiated with respect to η. 'Axial' equilibria have $\xi_E = 0$, and equilibrium values of η satisfy:

$$P'_4 = 4\alpha_4\eta^3 + 3\alpha_3\eta^3 + 2\alpha_2\eta + \alpha_1 = 0. \tag{16}$$

This equation may be rewritten as:

$$P'_4 = 4\alpha_4\{(\eta - w)^3 + u(\eta - w) + v\} = 0,$$

$$w = \frac{3\alpha_3}{4\alpha_4}, \quad u = \frac{\alpha_2}{2\alpha_4} - \tfrac{1}{3}w^2,$$

$$v = \frac{\alpha_1}{4\alpha_4} + \tfrac{1}{3}w\left[\tfrac{2}{9}w^2 - \frac{\alpha_2}{2\alpha_4}\right]. \tag{17}$$

The total number of axial equilibria can be one, two (one double root), or three depending on whether the index $4u^3 + 27v^2$ is positive, zero, or negative, respectively. 'Off-axial' equilibria ($\xi_E \neq 0$) are found by solving first for ξ as a function of η:

$$2\beta\xi^2 + P_2(\eta) = 0. \tag{18}$$

Clearly, off-axial equilibria will occur in pairs symmetrically placed about the η-axis. After substituting for ξ^2 in (15A), the following equation for equilibrium values of η results:

$$Q'_4 = P'_4 - \frac{1}{2\beta}P_2P'_2 = \omega_4\eta^4 + \omega_3\eta^3 + \omega_2\eta^2 + \omega_1\eta + \omega_0 = 0,$$

$$\omega_4 = \alpha_4 - \frac{1}{4\beta}\Omega_2^2, \quad \omega_3 = \alpha_3 - \frac{1}{2\beta}\Omega_1\Omega_2,$$

$$\omega_2 = \alpha_2 - \frac{1}{4\beta}[\Omega_1^2 + 2\Omega_0\Omega_2],$$

$$\omega_1 = \alpha_1 - \frac{1}{2\beta}\Omega_1\Omega_0, \quad \omega_0 = \alpha_0 - \frac{1}{4\beta}\Omega_0^2. \tag{19}$$

Admissible (ξ_E real) off-axial equilibria are constrained to the conic section (18). This conic intersects the η-axis if $P_2 = 0$ has real zeroes $\eta = \chi$ and $\eta = \zeta$. The intercepts coincide with these zeroes. Equation (19) may be rewritten as:

$$Q'_4 = 4\omega_4\{(\eta - \omega)^3 + \mu(\eta - \omega) + \nu\} = 0,$$

$$\omega = \frac{3\omega_3}{4\omega_4}, \quad \mu = \frac{\omega_2}{2\omega_4} - \tfrac{1}{3}\omega^2,$$

$$\nu = \frac{\omega_1}{4\omega_4} + \tfrac{1}{3}\omega\left[\tfrac{2}{9}\omega^2 - \frac{\omega_2}{2\omega_4}\right]. \tag{20}$$

If admissible, the total number of off-axial equilibrium pairs can be one, two (one pair of double roots), or three depending on whether the index $4\mu^3 + 27\nu^2$ is positive, zero, or negative, respectively. Axial and off-axial equilibrium values of η are known

analytic functions (roots of cubics) of the Hamiltonian coefficients. These coefficients are complicated functions (refer to Appendix A) of the average semimajor axis and polar angular momentum (parametric constants). Moreover, the numerical values of the Hamiltonian coefficients depend on the parameters modeling the gravitational field.

Infinitesimal stability of an equilibrium solution is determined by the eigenvalues $\bar{s}$ of Equations (14) linearized about an equilibrium point:

$$\bar{s} = \pm \frac{G_c}{L} \sqrt{\det \{H\}}, \quad \det \{H\} \triangleq \mathscr{H}_{\xi\eta}^2 - \mathscr{H}_{\xi\xi} \mathscr{H}_{\eta\eta}. \tag{21}$$

The Hessian determinant $\det\{H\}$ for axial equilibria is:

$$\det \{H\} = -2P_4''(\eta_A) P_2(\eta_A), \tag{22}$$

whereas for off-axial equilibria it is:

$$\det \{H\} = +4Q_4''(\eta_{OA}) P_2(\eta_{OA}). \tag{23}$$

Equilibria are stable (unstable) if the Hessian determinant is negative (positive).

For certain values of the Hamiltonian coefficients, the Hessian determinant can be identically zero. A small parametric variation in any or all of the Hamiltonian coefficients can render the determinant positive or negative. This signals a large qualitative change, or 'catastrophe' (after Thom, 1975), in the topology of phase plane trajectories near such an equilibrium. If the eigenvalues of the linearized system pass through zero, this will be called a *c*atastrophe of the *f*irst *k*ind, abbreviated 'CFK'. In addition to changing the stability of an equilibrium, CFK causes an increase or decrease in the total number of equilibria.

For the dynamical system under consideration, CFK can occur in three possible ways. Type I (denoted CFK(I)) occurs at equilibrium solutions which are double roots. Axial CFK(I) occurs if $4u^3 + 27v^2 = 0 (P_4'' = 0)$ whereas off-axial CFK(I) occurs if $4\mu^3 + 27v^2 = 0$ $(Q_4'' = 0)$. Type II, or CFK(II), occurs if an equilibrium solution coincides with one of the two real zeroes $\eta = \chi$ or $\eta = \zeta$ of $P_2 = 0$. Type III, or CFK(III), occurs if an equilibrium solution is a double root *and* if it coincides with χ or ζ. Axial CFK(III) occurs of $P_4'' = P_2 = 0$ whereas off-axial CFK(III) occurs if $Q_4'' = P_2 = 0$. Clearly, a necessary condition for CFK(II) and CFK(III) is that $P_2 = 0$ have *real* zeroes. As will be shown in Sections 4 and 5, each catastrophe type has trajectories with unique topology near the equilibrium point.

The averaged Hamiltonian (10), a constant of the motion by virtue of its autonomy, uniquely specifies ξ as a function of η. Such a trajectory is the locus of all points of intersection of a plane of constant $\mathscr{H} = \mathscr{H}_0$ with the two dimensional Hamiltonian surface in three space. The numerical value of $\mathscr{H}_0$ is determined by initial conditions. The explicit functional dependence of ξ on η is determined by the zeroes of the following biquadratic:

$$\beta\xi^4 + [P_2(\eta)]\xi^2 + [P_4(\eta) + \mathscr{H}_0] = 0,$$

$$\xi^2(\eta) = -\frac{1}{2\beta}P_2(\eta) \pm \sqrt{-\frac{1}{\beta}[Q_4(\eta) + \mathscr{H}_0]}. \tag{24}$$

Since all real solutions occur in pairs $(+\xi, -\xi)$, all trajectories are symmetric about the η-axis.

If two (or more) separatrices coalesce, this will be called a *c*atastrophe of the *s*econd *k*ind, abbreviated 'CSK'. As a result of coalescence, one separatrix passes through all of the equilibria associated with the individual separatrices before (or after) coalescence (see Figure 9 in Section 4). Separatrix coalescence is catastrophic because it dramatically alters the topological connectedness of the phase plane. In other words, changes occur in the relative sizes and shapes of domains of libration and circulation. For example, if two phase portraits which evolve from CSK (e.g., Figures 7 and 8 in Section 4) are compared, the same set of initial conditions in each can generate trajectories with significantly dissimilar features such as amplitude and frequency of libration. As in the case of CFK, parametric variation of the Hamiltonian coefficients can produce CSK.

Mathematically, CSK occurs if the Hamiltonian constants are equal for (at least) two unstable equilibria. Clearly, the same level curve of the Hamiltonian surface passes through each of these equilibria. For example, consider the negative Hamiltonians evaluated at an axial equilibrium η_A or an off-axial equilibrium η_{OA}:

$$-\mathscr{H}(0, \eta_A) = P_4(\eta_A), \quad -\mathscr{H}(\pm\xi_E, \eta_{OA}) = Q_4(\eta_{OA}). \tag{25}$$

If the quartic polynomial P_4 has three extrema, two of which are unstable, the numerical values of P_4 at the two unstable extrema are equal if $v = 0$. Similarly, if Q_4 has three extrema, two of which are admissible and unstable, CSK occurs if $v = 0$. Under certain other conditions, separatrices passing through axial and off-axial equilibria can coalesce. Moreover, CSK is possible with (at least) two CFK equilibria, provided these have separatrices, or with combinations of unstable and CFK equilibria.

4. A Two Parameter Family of Orbits Near Critical Inclination, Excluding Lunisolar Perturbations

A two parameter family is presented of orbits near critical inclination perturbed by the geopotential only. The two parameters are the average semimajor axis and polar angular momentum. All measured zonal harmonic coefficients from *G*oddard *E*arth *M*odel 10B, abbreviated 'GEM10B', are used. The numerical values of all 36 zonal harmonics appear in Table I, based on Lerch *et al.* (1978). Since lunisolar effects are *not* included, an upper semimajor axis limit of 3 Earth radii (abbreviated 'ER') is unnecessary. The results apply only to orbits with perigee heights above

TABLE I

GEM10B zonal harmonic coefficients
(based on Lerch *et al.*, 1978)

n	J_n
2	1.08263D-03
3	-2.53648D-06
4	-1.62330D-06
5	-2.26194D-07
6	5.42635D-07
7	-3.63286D-07
8	-2.07805D-07
9	-1.17254D-07
10	-2.41502D-07
11	2.28761D-07
12	-1.95500D-07
13	-2.22915D-07
14	1.24936D-07
15	-1.39194D-08
16	3.56163D-08
17	-9.28825D-08
18	-6.32607D-08
19	-1.06165D-08
20	-1.56877D-07
21	5.90169D-09
22	2.61620D-08
23	1.39855D-07
24	9.10000D-09
25	-2.85657D-09
26	-1.38322D-08
27	-4.82053D-08
28	1.09473D-07
29	5.06956D-08
30	1.24964D-08
31	5.55608D-09
32	5.80483D-08
33	3.11043D-08
34	6.22997D-08
35	-7.83632D-08
36	3.41760D-09

700 km because atmospheric drag is not modeled. Accordingly, for semimajor axes between 1 and 10 ER, the eccentricity ranges between 0.00 and 0.89.

The family is a collection of different (ξ, η) phase portraits for each point in a two dimensional parameter space with coordinates $(a, |H/L|)$. The absolute value of H/L is used because the results apply to prograde $(H > 0)$ and retrograde $(H < 0)$ critically inclined orbits. Each portrait is a collection of level curves of the averaged Hamiltonian, displaying the complicated interactions between eccentricity magnitude (the radial coordinate) and argument of perigee (the polar angle). Dynamical

fluctuations in eccentricity and inclination occur simultaneously such that polar angular momentum is conserved. Since the inclination is always close to critical ($(H/G_c)^2 = 1/5$), it is meaningful to define a 'critical' eccentricity e_c as a reference:

$$e_c = \sqrt{1 - 5(H/L)^2}. \tag{26}$$

A small annulus (maximum width $0(\sqrt{J_2})$ in eccentricity) centered on a circle of radius e_c is the 'resonance band'. Libration, characterized by long period oscillations in eccentricity and argument of perigee, can occur for initial conditions within the resonance band. Apsidal circulation (argument of perigee increasing or decreasing without bound) occurs outside the resonance band. Circulation is prograde, or in the direction of orbital motion, if $e > e_c (i < 63.4°$ or $i > 116.6°)$, and retrograde if $e < e_c$ $(63.4° < i < 116.6°)$, in agreement with elementary orbit theory.

The GEM10B parameter space (Figure 1) is subdivided into five *s*tructurally *s*tationary, abbreviated 'SS', subspaces: SS1, SS3A, SS5A, SS7A(i), and SS7A(ii). *Within* these subspaces, the stability and total number of phase portrait equilibria do not change, nor does separatrix coalescence occur. If the average semimajor axis and polar angular momentum are changed parametrically, quantitative changes in the phase portraits occur, such as frequency and amplitude of libration. The qualitative appearance of the portrait is the same. Physically, these parametric variations change the size of the orbit thereby redistributing the average orbit torque. Large qualitative changes in a phase portrait occur if the boundaries between subspaces are crossed. These include changes in stability and total number of equilibria (CFK), and separatrix coalescence (CSK).

SS1 portraits (Figure 2) have one stable axial equilibrium, and only prograde circulation PC. SS3A portraits (Figure 3) have three axial equilibria. The axial separatrix S through σ_1 resembles a plane polar geometric curve called a limacon. Unlike SS1, both prograde circulation (large e) and retrograde circulation RC (small e) occur. The asymmetry of SS1 and SS3A about the ξ-axis is due to the odd zonal harmonics. Axial CFK(I) portraits (Figure 4) are transitions between SS1 and SS3A. Separatrix topology is cuspodial near σ^* (a double root of (16)). Such a separatrix is characteristic of the appearance or disappearance of two axial equilibria with opposite stability.

SS5A portraits (Figure 5) have three stable axial equilibria and a pair of unstable off-axial equilibria. The off-axial separatrix S divides the SS5A phase plane into northern L_1 and southern L_2 hemispheric domains of libration. SS5A tends to be more symmetrical about the ξ-axis than SS3A, especially with increasing semimajor axis. The even zonal harmonics are less severely attenuated than the odd zonal harmonics within the parameter space region SS5A. CFK(II) portraits (Figure 6) are direct transitions between SS3A and SS5A, possible only if $e_c < 0.458$. In passing from SS5A to SS3A, two unstable off-axial equilibria λ_2 coalesce with one stable axial equilibrium σ_1 on the η-axis.

SS7A(i) portraits (Figure 7) and SS7A(ii) portraits (Figure 8) interrupt the direct

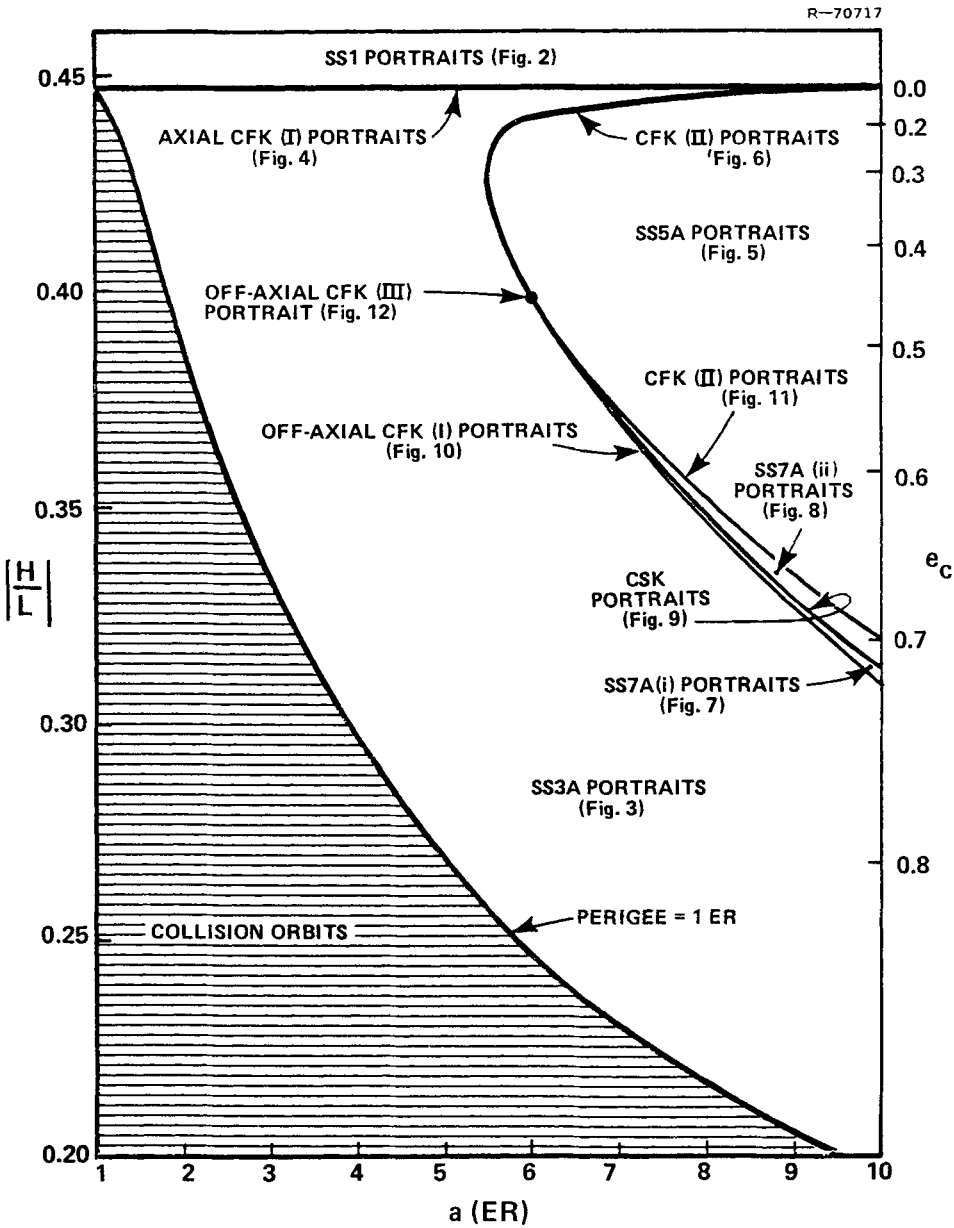

Fig. 1. The GEM10B parameter space, excluding lunisolar perturbations.

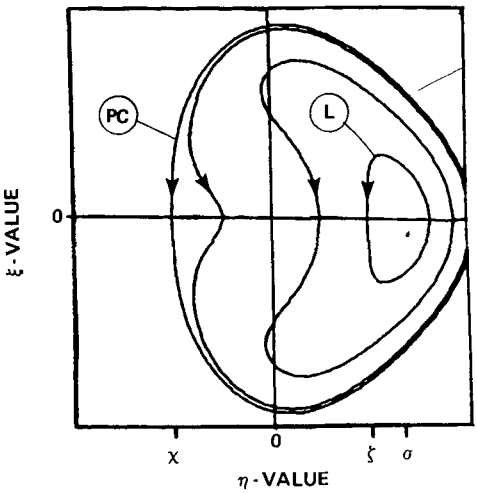

TRAJECTORY LABELS:
L : LIBRATION
PC : PROGRADE CIRCULATION

Fig. 2. SS1 portrait.

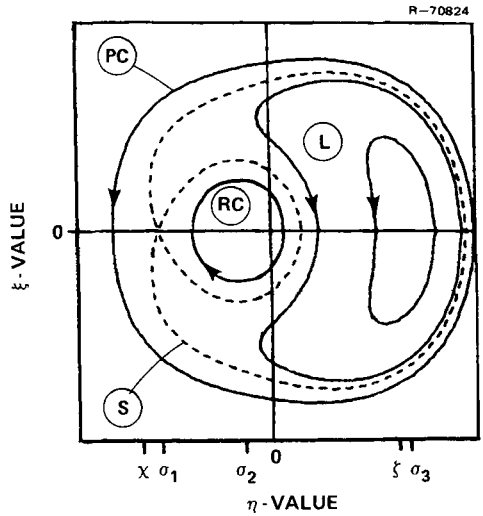

TRAJECTORY LABELS:
L : LIBRATION
S : AXIAL LIMACON SEPARATRIX
PC : PROGRADE CIRCULATION
RC : RETROGRADE CIRCULATION

Fig. 3. SS3A portrait.

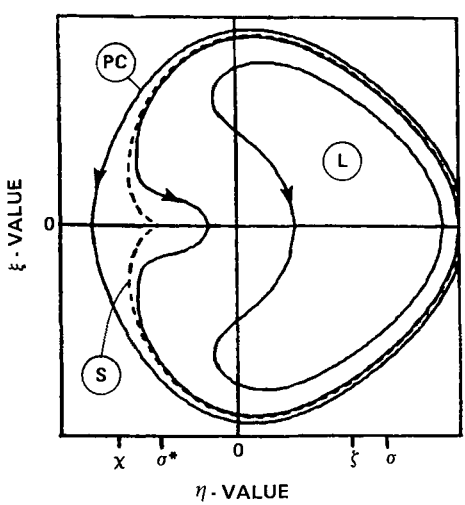

TRAJECTORY LABELS:
L : LIBRATION
S : AXIAL CFK (I) SEPARATRIX
PC : PROGRADE CIRCULATION

Fig. 4. Axial CFK(I) portrait.

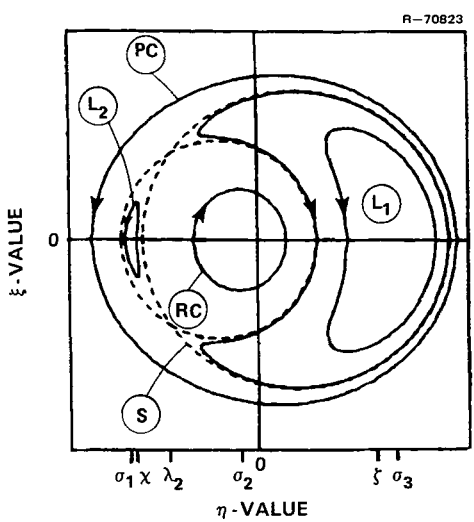

TRAJECTORY LABELS:
L_1 : NORTHERN AXIAL LIBRATION
L_2 : SOUTHERN AXIAL LIBRATION
S : SS5A SEPARATRIX
PC : PROGRADE CIRCULATION
RC : RETROGRADE CIRCULATION

Fig. 5. SS5A portrait.

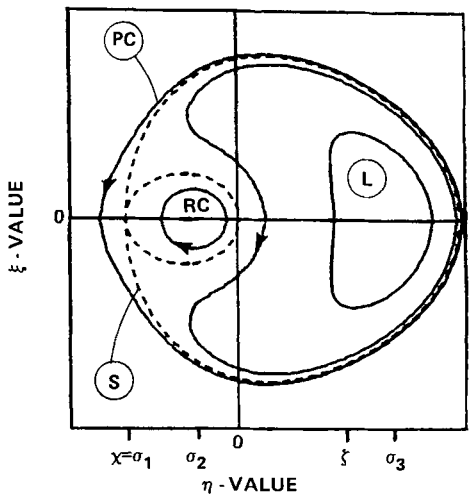

TRAJECTORY LABELS:
L : LIBRATION
S : CFK (II) SEPARATRIX
PC : PROGRADE CIRCULATION
RC : RETROGRADE CIRCULATION

Fig. 6. CFK(II) portrait.

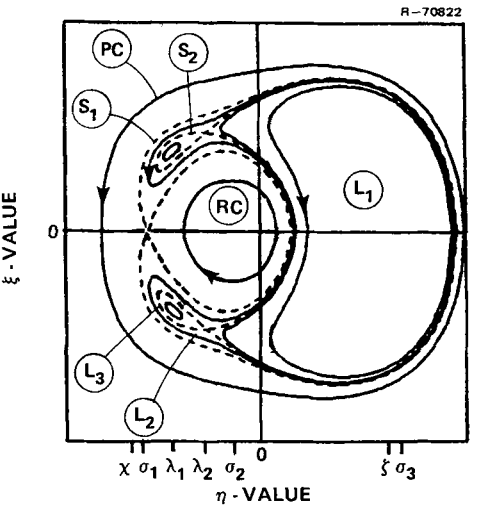

TRAJECTORY LABELS:
L_1 : INNERMOST AXIAL LIBRATION
L_2 : OUTERMOST AXIAL LIBRATION
L_3 : OFF-AXIAL LIBRATION
S_1 : AXIAL LIMACON SEPARATRIX
S_2 : OFF-AXIAL SEPARATRIX
PC : PROGRADE CIRCULATION
RC : RETROGRADE CIRCULATION

Fig. 7. SS7A(i) portrait.

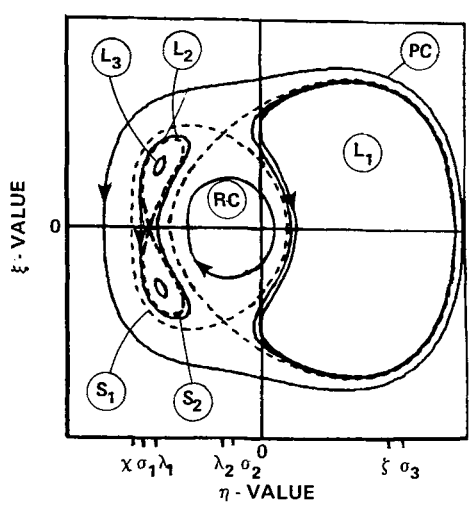

TRAJECTORY LABELS:
L_1 : NORTHERN AXIAL LIBRATION
L_2 : SOUTHERN AXIAL LIBRATION
L_3 : OFF-AXIAL LIBRATION
S_1 : OFF-AXIAL SEPARATRIX
S_2 : AXIAL LEMNISCATE SEPARATRIX
PC : PROGRADE CIRCULATION
RC : RETROGRADE CIRCULATION

Fig. 8. SS7A(ii) portrait.

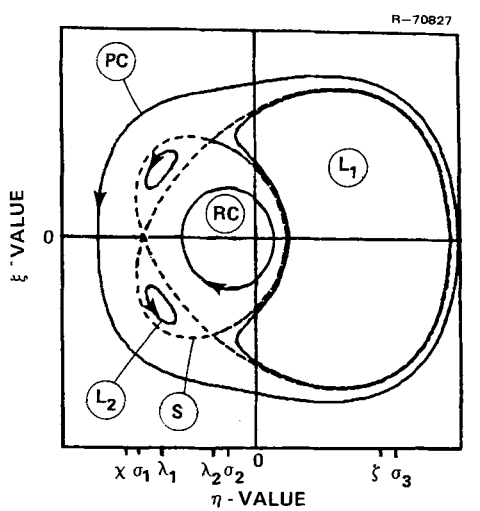

TRAJECTORY LABELS:
L_1 : AXIAL LIBRATION
L_2 : OFF-AXIAL LIBRATION
S : CSK (IC) SEPARATRIX
PC : PROGRADE CIRCULATION
RC : RETROGRADE CIRCULATION

Fig. 9. CSK portrait.

transition between SS3A and SS5A if $e_c > 0.458$. Although both have seven equilibria and two separatrices, they are topologically dissimilar. Compare, for example, librations labeled L_2 in both portraits. The amplitude of L_2 argument of perigee oscillations is much larger in SS7A(i) than in SS7A(ii). CSK portraits (Figure 9) are transitions between SS7A(i) and SS7A(ii). The CSK separatrix S passes through all of the unstable equilibria in the portrait. Unlike CFK, CSK does not cause a change in stability or a change in the total number of equilibria. Rather, CSK causes transfer of libration. For example, initial conditions near σ_1 in SS7A(i) predict libration L_2 about σ_3. The same initial conditions in SS7A(ii) predict libration L_3 about λ_1.

Off-axial CFK(I) portraits (Figure 10) are transitions between SS3A and SS7A(i). Separatrix topology is cuspoidal near λ^* (a double root of (18)). Such a separatrix is characteristic of the appearance or disappearance of two pairs of off-axial equilibria with opposite stabilities. A new CFK(II) portrait (Figure 11) separates SS5A and SS7A(ii). In the transition SS7A(ii) to SS5A, two stable off-axial equilibria λ_1 coalesce with one unstable axial equilibrium σ_1 on the η-axis.

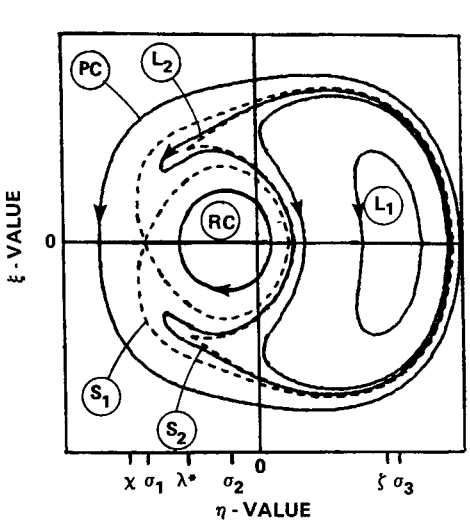

TRAJECTORY LABELS:

L_1 : INNERMOST AXIAL LIBRATION

L_2 : OUTERMOST AXIAL LIBRATION

S_1 : AXIAL LIMACON SEPARATRIX

S_2 : OFF-AXIAL CFK (I) SEPARATRIX

PC : PROGRADE CIRCULATION

RC : RETROGRADE CIRCULATION

Fig. 10. Off-axial CFK(I) portrait.

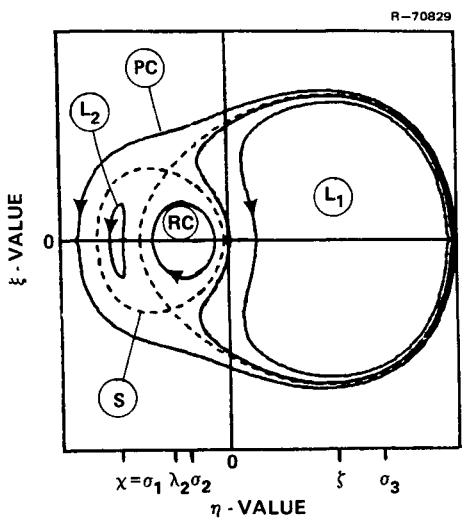

TRAJECTORY LABELS:

L_1 : NORTHERN AXIAL LIBRATION

L_2 : SOUTHERN AXIAL LIBRATION

S : OFF-AXIAL SEPARATRIX

PC : PROGRADE CIRCULATION

RC : RETROGRADE CIRCULATION

Fig. 11. CFK(II) portrait.

The foregoing results agree qualitatively with similar results reported by Jupp (1975). For purposes of comparison, regions SS3A, SS5A, SS7A(i) and SS7A(ii) correspond to Jupp's cases (1), (3), (2.2), and (2.3), respectively. Off-axial CFK(I) and CSK correspond to Jupp's loci $h_0 h_2 = 1$ and $R = 0$, respectively. The entire CFK(II) boundary corresponds to Jupp's locus $h_0 + h_2 = 1$. Some significant quantitative differences exist. For example, compare the parameter space coordinates of off-axial CFK(III) portraits (Figure 12). Jupp would have predicted CFK(III) at $e_c = \sqrt{6/13}$ (independent of Earth model) and semimajor axis 3.960 ER (using GEM10B). It is worth noting that Jupp truncated his second-order long period Hamiltonian at J_5 and e^3. When zonal harmonics J_6 through J_{36} and e^4 terms are included, CFK(III) shifts to $e_c = 0.458$ and semimajor axis 6.011 ER (Figure 1). A sensitivity analysis shows that, of all the 36 harmonics modeled, the zonal harmonics J_6 through J_9 are the primary contributors to this shift. Of these, J_6 caused the most significant departure from Jupp's numerical predictions (see also Jupp, 1980). Lunisolar perturbations cause even more drastic alterations of these results (refer to Section 5).

The axial equilibrium σ_3 is stable throughout the parameter space. The periods of small oscillations near σ_3 are of the order of 100 yrs for semimajor axes less than

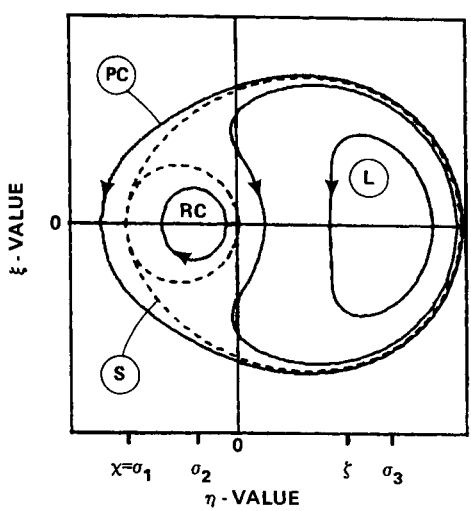

TRAJECTORY LABELS:

L : LIBRATION

S : OFF-AXIAL CFK (III) SEPARATRIX

PC : PROGRADE CIRCULATION

RC : RETROGRADE CIRCULATION

Fig. 12. Off-axial CFK(III) portrait.

2 ER. These librations get slower with increasing semimajor axis due to the attenuation of the zonal harmonic restoring torques. At a semimajor axis of 10 ER, libration periods decrease from 10^6 yrs at $e_c = 0.25$ to 10^4 yrs at $e_c = 0.83$ because restoring torque amplitudes grow with decreasing perigee height. Small oscillations within the resonance band are clearly much slower than any of the periodic fluctuations averaged out of the long period Hamiltonian.

The tolerance is extremely small on initial conditions which predict such librations. A measure of this tolerance is the maximum radial separation of two branches of a separatrix (usually at η-axis crossings). For example, at a semimajor axis of 2 ER and for an initial argument of perigee of 90°, libration occurs if the initial eccentricity is 0.200 ± 0.016. For a semimajor axis of 5 ER, libration occurs if the initial eccentricity is 0.200 ± 0.005. It is clear that the maximum change in eccentricity is small (as predicted by Garfinkel, 1960), justifying the linearization of the Hamiltonian about e_c (refer to Section 2).

5. A Two Parameter Family of Orbits Near Critical Inclination, Including Lunisolar Perturbations

A two parameter family is presented of orbits near critical inclination perturbed by the geopotential with lunisolar effects included. The two parameters are the average semimajor axis and polar angular momentum. Earth model GEM10B is used. Atmospheric drag is not included. Semimajor axes between 1 and 3 ER, and eccentricities between 0.00 and 0.63 are considered.

Lunisolar perturbations considerably modify the appearance of the GEM10B parameter space (Figure 13). Four structurally stationary regions are observed: SS1, SS3A, SS5A, and SS3B. (SS5A occupies the remainder of the parameter space between $|H/L| = 0.420$ and the collision orbit boundary (not shown).) Although SS1, SS3A, and SS5A reappear, the direct transition between SS3A and SS5A occurs for orbits with semimajor axes *less* than 1.556 ER, and for eccentricities greater than 0.040. SS3B is a new region created by the lunisolar perturbations. A direct transition between SS3B and SS5A is possible for semimajor axes greater than 1.556 ER and eccentricities greater than 0.040. Phase portraits in all four regions have but one separatrix each, precluding CSK for semimajor axes less than 3 ER.

Off-axial CFK(III) occurs at $e_c = 0.316$ and semimajor axis 1.421 ER (a collision orbit, not shown in Figure 13), provided zonal harmonics J_8 through J_{36} are *not* included. It is noteworthy that, for this Earth model, Jupp would have predicted off-axial CFK(III) at $e_c = 0.679$ and semimajor axis 3.960 ER without the Sun and Moon. Under those conditions for which off-axial CFK(III) is observed, regions SS7A(i) and SS7A(ii) as well as CSK would occur for larger eccentricity ($e > 0.316$) collision orbits.

SS1 portraits (Figure 2) are precluded for semimajor axes greater than 1.8 ER because the Sun and Moon destabilize the origin of the (ξ, η) phase plane. For semi-

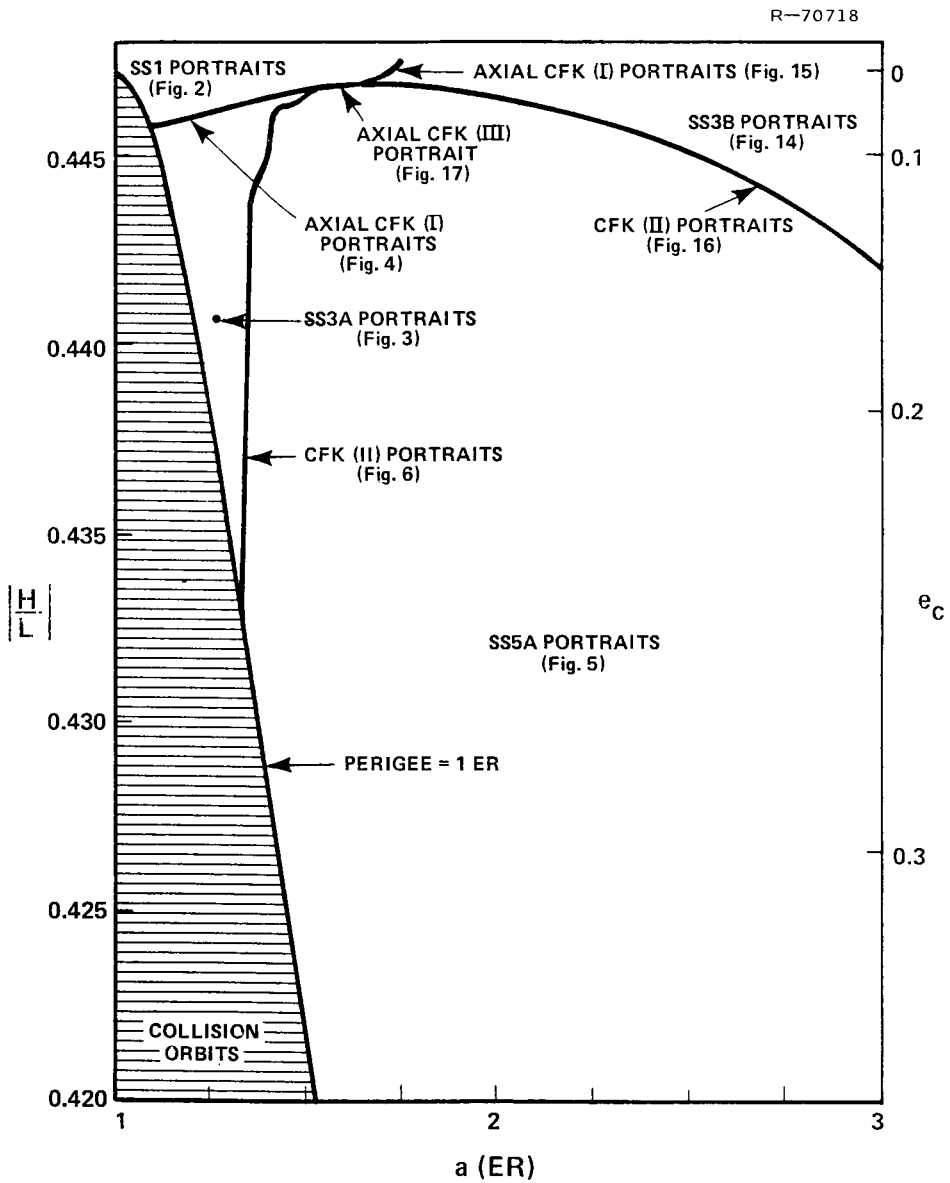

Fig. 13. The GEM10B parameter space, including lunisolar perturbations.

major axes less than 1.4 ER and $e_c = 0.1$ or larger, torques arising from odd order zonal harmonics destabilize σ_1, creating asymmetrical SS3A portraits (Figure 3). With increasing semimajor axis, lunisolar torques assist the even order zonal harmonics in stabilizing σ_1, creating SS5A portraits (Figure 5) and SS3B portraits (Figure 14). Each has a northern L_1 and a southern L_2 hemispheric domain of libration. Due to the lunisolar effects, SS5A and SS3B portraits become more symmetrical about

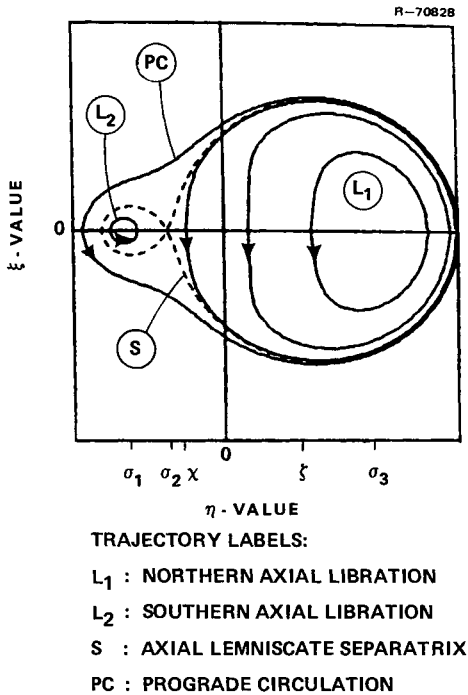

Fig. 14. SS3B portrait.

the ξ-axis as the semimajor axis is increased. Moreover, any admissible off-axial equilibria in SS3B are precluded. Note that the equilibrium σ_2 is unstable (Figure 14) because it is close to the origin of the phase plane. The SS3B separatrix S passing through σ_2 resembles a plane polar geometric curve called a lemniscate. Outside the lemniscate, circulatory apsidal motion PC is always prograde.

Axial CFK(I) portraits (Figure 15) are transitions between SS1 and SS3B. The CFK separatrix S has a cusp whose pointed end is convex toward negative η. This feature distinguishes Figure 15 from Figure 4, also an axial CFK(I) portrait. In the transition between SS1 and SS3A (Figure 4), the separatrix cusp is convex toward positive η. Either transition, SS3B to SS1 or SS3A to SS1, causes the two axial equilibria σ_1 and σ_2 to coalesce. If σ_1 is stable whereas σ_2 is unstable, Figure 15 results. If σ_1 is unstable whereas σ_2 is stable, Figure 4 results.

CFK(II) portraits (Figure 16) are transitions between SS3B and SS5A. The CFK separatrix S has two circular branches which are tangent to each other at σ_2. This feature distinguishes Figure 16 from Figure 6, also a CFK(II) portrait. In the transition between SS3A and SS5A (Figure 6), the separatrix branches are tangent at σ_1. Either transition, SS5A to SS3B or SS5A to SS3A, causes a pair of unstable off-axial equilibria to coalesce with one stable axial equilibrium, forming the point of tangency of the two separatrix branches.

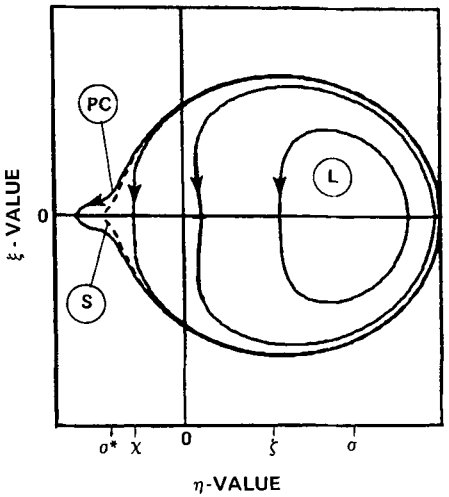

TRAJECTORY LABELS:

L : LIBRATION

S : AXIAL CFK (I) SEPARATRIX

PC : PROGRADE CIRCULATION

Fig. 15. Axial CFK(I) portrait.

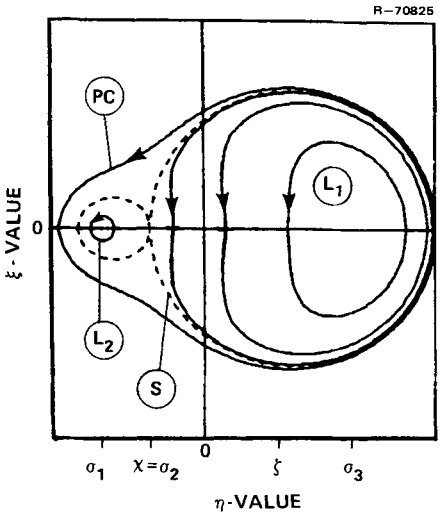

TRAJECTORY LABELS:

L_1 : NORTHERN AXIAL LIBRATION

L_2 : SOUTHERN AXIAL LIBRATION

S : CFK (II) SEPARATRIX

PC : PROGRADE CIRCULATION

Fig. 16. CFK(II) portrait.

The CFK(I) and CFK(II) parameter space boundaries are mutually tangent at $e_c = 0.040$ and semimajor axis 1.556 ER, creating an axial CFK(III) portrait (Figure 17). The transition from SS5A to SS1 through axial CFK(III) causes a pair of unstable off-axial equilibria λ_2 and a pair of stable axial equilibria σ_1 and σ_2 to coalesce at σ^*. This portrait is quite dissimilar to an off-axial CFK(III) portrait (Figure 12), the latter precluded by the inclusion of the lunisolar perturbations.

The axial equilibrium σ_3 is stable throughout the parameter space. Small oscillations near σ_3 are slowest (250 yrs) for e_c close to zero and semimajor axes between 1.7 and 2.1 ER. Faster oscillations are observed with increasing semimajor axis due to the amplification of the lunisolar restoring torque. (The zonal harmonic torque attenuates.) At a semimajor axis of 3 ER, libration periods decrease from 150 years at $e_c = 0.06$ to 100 yrs at $e_c = 0.21$. The zonal harmonic restoring torque amplifies with decreasing perigee height, and the lunisolar torque amplifies with increasing apogee height. Highly eccentric orbits with semimajor axis 3 ER exhibit oscillatory periods of 18.6 yrs, commensurate with lunar nodal precession. It is therefore anticipated that periodic lunar gravity gradient torques can disrupt perigee resonance, necessitating a separate treatment.

Equilibrium inclinations begin to differ significantly from the critical values 63.4°

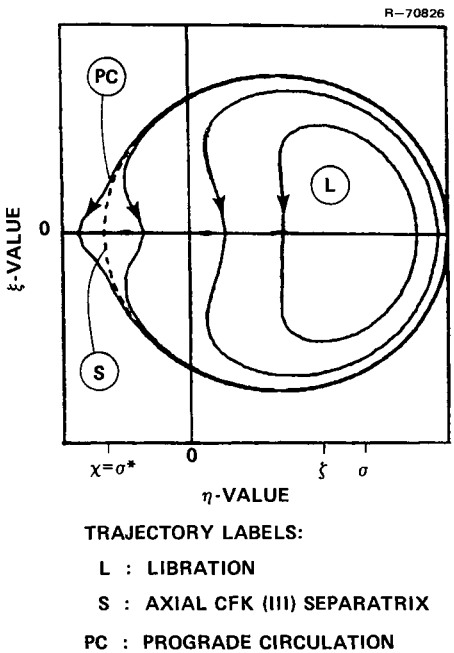

Fig. 17. Axial CFK(III) portrait.

and 116.6° as the semimajor axis is increased. Moreover, with the lunisolar perturbations included, the tolerance is larger on initial conditions which predict libration. For example, at a semimajor axis of 3 ER and for an initial argument of perigee of 90°, equilibrium inclinations are 63.1° for prograde orbits and 116.9° for retrograde orbits. Liberation can occur if the initial eccentricity is 0.10 ± 0.10. These trends suggest that the Hamiltonian cannot be linearized about inclinations 63.4° or 116.6° because, with the Sun and Moon included, the critical inclination changes with increasing semimajor axis.

For semimajor axes between 3 and 6 ER, the dominant perturbations affecting the long period motion of perigee are Earth oblateness and the lunisolar gravity gradient. For inclinations away from 63.4° and 116.6°, the oblateness effect on apsidal motion is clearly much more significant than higher order zonal harmonics. With increasing semimajor axis, the lunisolar effects amplify while the higher order zonal harmonics attenuate. Since oblateness forces also attenuate, the Sun and Moon effects become as large as oblateness near synchronous altitudes. Consequently, Earth oblateness and lunisolar gravity must both be treated as first-order effects at high altitudes.

6. Summary and Conclusions

Orbits near the critical inclinations 63.4° and 116.6° exhibit long period fluctuations in perigee distance and angular location of perigee (perigee resonance). Since the

average perigee location is unchanged by Earth oblateness at the critical inclinations, perigee resonance is caused by North-South gravitational forces due to the Earth's distortion from an oblate spheroid, the Moon and the Sun. Non-gravitational forces caused by atmospheric drag and solar radiation pressure can disrupt perigee resonance, but these effects were not modeled. Drag could be neglected for orbits with perigee altitudes above 700 km. Solar radiation pressure effects will be examined in a future paper dealing with Sun synchronous orbits near the critical inclination 116.6°.

Phase portraits were used to depict perigee resonance. The Hamiltonian constant was chosen as the parameter to display a family of phase plane trajectories consisting of libration, circulation, and asymptotic motion along separatrices near equilibrium points. A two parameter family of phase portraits was defined by two other integrals of motion, the average semimajor axis and polar angular momentum. Large qualitative changes in phase portrait topology occurred when the total number and infinitesimal stability of equilibria changed, or when two separatrices coalesced. These changes occurred abruptly despite continuous parametric variation in one or more of the integrals of motion.

Two families of phase portraits were compared to illustrate the significant impact of the lunisolar perturbations. Without lunisolar effects, certain phase portraits with seven equilibria where predicted for eccentricities exceeding 0.458 and semimajor axes greater than 6.011 Earth radii. These predictions agreed qualitatively but not quantitatively (due to J_6) with similar results first reported by Jupp (1975). With lunisolar effects included, Jupp's phase portraits reappeared, but for collision orbits only. Lunisolar gravity was shown to control stability and the total number of phase plane equilibria for orbits with semimajor axes exceeding 1.4 Earth radii. With increasing semi-major axis, the physical properties of stable perigee motions changed significantly. Periods of small oscillations ranged between 250 yrs and 20 yrs. Maximum possible fluctuations in eccentricity about equilibrium were $\pm 100\%$ at a semimajor axis of 3 Earth radii.

Acknowledgements

I would like to thank my adviser, John V. Breakwell from Stanford University, for suggesting this problem and for helping me solve it. I also thank Daniel B. DeBra, J. David Powell, Alan H. Jupp, and Boris Garfinkel for their helpful suggestions.

Appendix A: The Second-Order Hamiltonian Coefficients

Analytic expressions for the second-order Hamiltonian coefficients are presented.

Define the parameter:

$$\bar{J}_n = J_n \left(\frac{R_\oplus}{a} \right)^n, \tag{27}$$

where J_n is a zonal harmonic coefficient of order n. The satellite orbit semimajor axis is denoted by 'a' and $R_\oplus$ is the radius of the Earth. Also define:

$$\lambda_{\odot\mathfrak{C}} = \left[\frac{\mu_\odot}{\mu_\oplus}\left(\frac{R_\oplus}{a_\odot}\right)^3 + \frac{\mu_\mathfrak{C}}{\mu_\oplus}\left(\frac{R_\oplus}{a_\mathfrak{C}}\right)^3 P_2(C(\varepsilon_\mathfrak{C}))\right] P_2(C(\varepsilon)),$$

$$\nu_\mathfrak{C} = \frac{\mu_\mathfrak{C}}{\mu_\oplus}\left(\frac{R_\oplus}{a_\mathfrak{C}}\right)^5 P_4(C(\varepsilon)) P_4(C(\varepsilon_\mathfrak{C})), \tag{28}$$

where $\mu_\oplus, \mu_\mathfrak{C}$, and $\mu_\odot$ are the gravitational parameters of the Earth, Moon, and Sun respectively. The semimajor axes of the Moon's orbit and the apparent solar orbit are denoted by $a_\mathfrak{C}$ and $a_\odot$. The symbol ε is the obliquity of the ecliptic, and $\varepsilon_\mathfrak{C}$ is the ecliptic inclination of the lunar orbit plane. P_2 and P_4 are Legendre polynomials, not to be confused with other polynomials with the same symbols appearing in Section 3. The numerical values of $\lambda_{\odot\mathfrak{C}}$ and $\nu_\mathfrak{C}$ are 6.2×10^{-8} and 4.7×10^{-12} (dimensionless), respectively.

The second-order secular coefficients A_{00}, A_{20}, and A_{40} contain higher even order zonal harmonics and lunisolar perturbations:

$$A_{00}(L, G, H) = \bar{\varphi}_2(L, G, H) + \sum_{n \geq 4 \text{ EVEN}} \bar{J}_n \left(\frac{L}{G}\right)^{2n-1} F_{n,n/2}(G, H) -$$

$$- \tfrac{1}{4}\lambda_{\odot\mathfrak{C}}\left(\frac{a}{R_\oplus}\right)^3 P_2(C(i)) - \tfrac{9}{64}\nu_\mathfrak{C}\left(\frac{a}{R_\oplus}\right)^5 P_4(C(i)), \tag{29}$$

$$A_{20}(L, G, H) = -\sum_{n \geq 4 \text{ EVEN}} \bar{J}_n \left(\frac{L}{G}\right)^{2n-1} \binom{n-1}{2} F_{n,n/2}(G, H) +$$

$$+ \tfrac{3}{4}\lambda_{\odot\mathfrak{C}}\left(\frac{a}{R_\oplus}\right)^3 P_2(C(i)) + \tfrac{45}{32}\nu_\mathfrak{C}\left(\frac{a}{R_\oplus}\right)^5 P_4(C(i)), \tag{30}$$

$$A_{40}(L, G, H) = -\frac{3}{8}\sum_{n \geq 6 \text{ EVEN}} \bar{J}_n \left(\frac{L}{G}\right)^{2n-1} \binom{n-1}{4} F_{n,n/2}(G, H) +$$

$$+ \tfrac{135}{512}\nu_\mathfrak{C}\left(\frac{a}{R_\oplus}\right)^5 P_4(C(i)), \tag{31}$$

L, G, and H are DeLaunay momenta. F_{nq} is a form of Kaula's inclination function (Kaula, 1966) adapted for zonal harmonics:

$$F_{n,q}(G, H) = 2\sum_{j=0}^{q^*} (-1)^j \binom{n-2j}{q^*-j} T_{nj}\left[1 - \left(\frac{H}{G}\right)^2\right]^{(n-2j)/2}$$

$$T_{nj} = \frac{(2n-2j)!}{2^{2n-2j} j!(n-j)!(n-2j)!}$$

$$q^* = \tfrac{1}{2}(n-q). \tag{32}$$

$\bar{\varphi}_2$ is the Von Zeipel correction to the second-order secular term (Brouwer and Clemence, 1961):

$$\bar{\varphi}_2(L, G, H) = -\tfrac{1}{4}\bar{J}_2^2\left\{\frac{3}{32}\left(\frac{L}{G}\right)^5\left[5 - 18\left(\frac{H}{G}\right)^2 + 5\left(\frac{H}{G}\right)^4\right] + \right.$$
$$+\frac{3}{8}\left(\frac{L}{G}\right)^6\left[1 - 6\left(\frac{H}{G}\right)^2 + 9\left(\frac{H}{G}\right)^4\right] -$$
$$\left. -\frac{15}{32}\left(\frac{L}{G}\right)^7\left[1 - 2\left(\frac{H}{G}\right)^2 - 7\left(\frac{H}{G}\right)^4\right]\right\}. \tag{33}$$

The second-order long period coefficients B_{11}, B_{31}, and B_{33} contain only higher odd order zonal harmonics:

$$B_{11}(L, G, H) = -\sum_{n \geq 3 \text{ ODD}} \tfrac{1}{2}(n-1)\bar{J}_n\left(\frac{L}{G}\right)^{2n-1} F_{n,(n-1)/2}(G, H), \tag{34}$$

$$B_{31}(L, G, H) = -\sum_{n \geq 5 \text{ ODD}} \tfrac{1}{8}(n-1)(n-2)(n-3)\bar{J}_n\left(\frac{L}{G}\right)^{2n-1} F_{n,(n-1)/2}(G, H), \tag{35}$$

$$B_{33}(L, G, H) = -\sum_{n \geq 5 \text{ ODD}} \tfrac{1}{24}(n-1)(n-2)(n-3)\bar{J}_n\left(\frac{L}{G}\right)^{2n-1} \times$$
$$\times F_{n,(n-3)/2}(G, H). \tag{36}$$

The second-order long period coefficients C_{22}, C_{42}, and C_{44} contain higher even order zonal harmonics and lunisolar perturbations:

$$C_{22}(L, G, H) = -\sum_{n \geq 4 \text{ EVEN}} \tfrac{1}{4}(n-1)(n-2)\bar{J}_n\left(\frac{L}{G}\right)^{2n-1} F_{n,(n-2)/2}(G, H) -$$
$$-\tfrac{3}{64}\bar{J}_2^2\left(\frac{L}{G}\right)^7\left[1 - 16\left(\frac{H}{G}\right)^2 + 15\left(\frac{H}{G}\right)^4\right] -$$
$$-\tfrac{5}{16}\lambda_{\odot\mathbb{C}}\left(\frac{a}{R_\oplus}\right)^3 P_{22}(C(i)) - \tfrac{21}{256}\nu_{\mathbb{C}}\left(\frac{a}{R_\oplus}\right)^5 P_{42}(C(i)), \tag{37}$$

$$C_{42}(L, G, H) = -\sum_{n \geq 6 \text{ EVEN}} \tfrac{1}{48}(n-1)(n-2)(n-3)(n-4)\bar{J}_n\left(\frac{L}{G}\right)^{2n-1} \times$$
$$\times F_{n,(n-2)/2}(G, H) - \tfrac{21}{512}\nu_{\mathbb{C}}\left(\frac{a}{R_\oplus}\right)^5 P_{42}(C(i)), \tag{38}$$

$$C_{44}(L, G, H) = -\sum_{n \geq 6 \text{ EVEN}} \tfrac{1}{192}(n-1)(n-2)(n-3)(n-4)\bar{J}_n\left(\frac{L}{G}\right)^{2n-1} \times$$
$$\times F_{n,(n-4)/2}(G, H) + \tfrac{63}{4096}\nu_{\mathbb{C}}\left(\frac{a}{R_\oplus}\right)^5 P_{44}(C(i)), \tag{39}$$

where P_{42} and P_{44} are Legendre functions. The Von–Zeipel correction to the second-order long period term, taken from Brouwer and Clemence (1961), is incorporated in C_{22}.

References

Aoki, S.: 1963a, *Astron. J.* **68**, 355.

Aoki, S.: 1963b, *Astron. J.* **68**, 365.

Brouwer, D. and Clemence, G.: 1961, *Methods of Celestial Mechanics*, Academic Press, New York, N.Y.

Garfinkel, B.: 1960, *Astron. J.* **65**, 624.

Garfinkel, B.: 1973, *Celes. Mech.* **8**, 25.

Giacaglia, G.: 1973, *Lunar Perturbations of Artificial Satellites of the Earth*, Smithsonian Astrophysical Observatory, Cambridge, MA., SAO SR-352.

Hagihara, Y.: 1961, *Smithsonian Contrib. Astrophys.* **5**.

Hensley, D. and Breakwell, J.: 1967, *First Compilation of Papers on Trajectory Analysis and Guidance Theory*, National Aeronautics and Space Administration, Washington, D.C., NASA SP-141.

Hori, G.: 1960, *Astron. J.* **65**, 291.

Jupp, A.: 1975, *Celes. Mech.* **11**, 361.

Jupp, A.: 1980, *Celes. Mech.* **21**, 361.

Kaula, W.: 1966, *Theory of Satellite Geodesy*, Blaisdell Pub. Co., Waltham, MA.

Kozai, Y.: 1961, *Smithsonian Contrib. Astrophys.* **5**, No. 5.

Kozai, Y.: 1973, *A New Method to Compute Lunisolar Perturbations in Satellite Motions*, Smithsonian Astrophysical Observatory, Cambridge, MA., SAO SR-349.

Lange, B., DeBra, D., and Kaula, W.: 1969, *A Preliminary Design of a Drag-Free Satellite and Its Application to Geodesy*, NASA Electronics Research Center, Cambridge, MA., Report No. NAS-12-695 (Final Report).

Lerch, F. and Wagner, C. *et al.*: 1978, 'Gravity Model Improvement Using GEOS-3 Altimetry (GEM 10A and 10B)', *Proceedings of the 1978 Spring Annaul Meeting of the American Geo-physical Union*, Miami, Fla.

Petty, C. and Breakwell, J.: 1960, *Journal of the Franklin Institute* **270**, 259.

Thom, R.: 1975, *Structural Stability and Morphogenesis*, Benjamin Co., New York, N. Y. English translation by D. H. Fowler.

Vagners, J.: 1967, *Some Resonant and Non-Resonant Perturbations of Earth and Lunar Orbiters*, Dept. of Aeronautics and Astronautics, Stanford University, Stanford, CA., SUDAAR No. 317.